Nonlinear synthesis of input signals in ultrasonic experimental setups

Frédéric Conil,[a] Dominique Gibert,[b] and Florence Nicollin[c]
Géosciences Rennes (CNRS UMR 6118), Université Rennes 1, Bât. 15 Campus de Beaulieu, 35042 Rennes cedex, France

(Received 21 April 2003; revised 12 August 2003; accepted 15 August 2003)

A method is proposed to find the digital input signals to enter in nonlinear acoustical systems (power amplifiers, transducers, etc.) in order to obtain desired arbitrary response signals. The searched input signals are found by performing a Monte Carlo search guided by a simulated annealing process applied to a hidden model with a small number of parameters. The physical system is actually used in the optimization procedure, in a real-time manner, so that no theoretical model of the system response is required. The main aspects of the algorithm are described and illustrated with several examples. © *2004 Acoustical Society of America.* [DOI: 10.1121/1.1618241]

PACS numbers: 43.58.Vb, 43.58.Ry, 43.60.Mn [EJS] Pages: 246–252

I. INTRODUCTION

The design and the control of the signals emitted and received during acoustical experiments is an important issue in many situations. Indeed, the information of interest is often contained in tiny features present in the received signals and defined with respect to reference signals recorded in calibration experiments. Such changes may, for instance, be small amplitude or phase changes, dispersion effects, time delays, etc. In all cases, the better the control of the reference signals, the better the signal-to-noise ratio and the quality of the information. A popular approach followed in many experiments consists in using impulse input signals with a large bandwidth and to performing a deconvolution of the recorded signals in order to reduce the response signals into the time responses which would be obtained for a Dirac $\delta(t)$ entered in the system. A complementary dual technique consists in entering the system with sinusoidal input signals in order to obtain the response in the frequency domain. Both approaches assume that the whole system, i.e., the acoustical apparatus plus the studied physical system, is linear so that the superposition principle is valid (e.g., Bendat and Piersol, 1971). However, there remain many instances where acoustical setups operate nonlinearly out of their nominal ranges. This is frequent in geophysics and physical oceanography where high acoustical power is necessary to insonify remote targets or deep geological layers in tomography experiments and seafloor imaging. In such cases both the piezoelectric transducers and the power amplifiers have nonlinear responses which may considerably complicate laboratory post-processing operations [Fig. 1(a)]. Classical instrumental deconvolution and mode superposition can no more be used to process these nonlinear transfer functions. Waveform distortions can also be produced by nonlinear propagation of sound in water. In some instances, these distortions may need corrections although they mainly occur for long propagation distances. Even when operating in the linear domain, deconvolution operations remain a delicate task because of their fundamental ill-posedness and of their lack of robustness with respect to noise (Jurkevics and Wiggins, 1984). Hence, in delicate high-precision experiments where instrumental responses have to be carefully controlled, deconvolution may become a limiting factor because of an insufficient numerical precision.

In recent experiments (Le Gonidec, 2001; Le Gonidec *et al.*, 2002, 2003; Gautier, 2002; Gautier and Gibert, 2003), we used an alternative approach where the nonlinear response of the whole apparatus is accounted for in a preliminary reference experiment. This is done by searching for the input signals $s(t)$ to enter into the power amplifier, triggering the acoustical source such that the corresponding response signals $r(t)$ recorded by the receiving transducers satisfy *a priori* imposed constraints (Fig. 2). These constraints may take various forms such as, for instance, a prescribed shape for $r(t)$, a maximum time duration, a controlled spectral content, an imposed regularity, etc. The principal advantage of this method is that no further processing is needed in the remaining experiments, and data with both a high signal-to-noise ratio and a good time resolution can be acquired in a real time manner. In order to account for a possibly very nonlinear distorting behavior of the system (especially the source line) the proposed algorithm uses a fully nonlinear optimization method based on simulated annealing. A key point of the method is that the whole physical system is actually included in the optimization procedure so that no theoretical model of the system response is needed. In opposition to most inverse problems whose dual direct problems are numerically solved, the forward problem considered in the present study is the physical system by itself, i.e., the whole acoustical setup composed of arbitrary waveform generators, power amplifiers, piezoelectric transducers, water tank, A/D converters, etc. By this way, the sought input signals are found by directly using the real system whatever its response, which indeed may remain unknown. This approach differs from more traditional optimization algorithms which need a model of the system response (e.g., Trucco, 2002).

[a]Electronic mail: frederic.conil@univ-rennesl.fr
[b]Author to whom correspondence should be addressed. Electronic mail: dominique.gibert@univ-rennes1.fr
[c]Electronic mail: florence.nicollin@univ-rennes1.fr

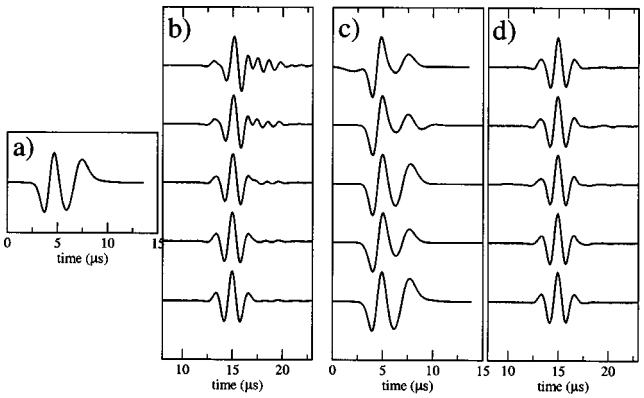

FIG. 1. Examples of nonlinear responses observed with two piezoelectric transducers immersed in a water tank (see Fig. 2). (a) Input signal sent by the arbitrary waveform generator. (b) Response signals obtained by progressively increasing (from bottom to top) the power of the source unit. The larger the source power, the more the nonlinear distortions in the late part of the received signals. (c) Input signals obtained by simulated annealing and constrained to produce response signals (d) with a prescribed shape for the same source powers as in (b). For clarity, all signals have their maximum value normalized to 1.

The high-speed electronic and computerized devices available today make it possible to plug in experimental setups into nonlinear inversion algorithms like simulated annealing. One objective of this paper is to show that nonlinear algorithms like simulated annealing, which need to solve the forward problem a huge number of times, can now be used to optimize routine experiments in a reasonable delay.

II. METROPOLIS ALGORITHM AND SIMULATED ANNEALING

A. Numerical modeling of input signals

Simulated annealing is an intensive iterative stochastic method which tests a large number of input signals $s(t)$ in order to progressively converge toward an optimal solution. The number of signals to be tested is proportional to the combinatorial complexity of the problem at hand which depends on the number of unknown parameters to optimize. For instance, a direct search of the $M=1024$ first values of an 8-bit discretized input signal results in a 256^{1024} combinatorial complexity, implying to test a too huge number of input signals to warrant a convergence toward well-optimized solutions in a reasonable delay. In the present study, we reduce the dimensionality of the optimization problem by writing the input signal as a linear combination of elementary functions $\Psi_j(t)$ parametrized with three quantities, namely, the amplitude A_j, the dilation a_j, and the time position t_j which are the unknown parameters to estimate. Practically, this reads

$$s(t|\mathbf{m})=\sum_{j=1}^{N} A_j \Psi\left(\frac{t-t_j}{a_j}\right), \tag{1}$$

where N is the total number of elementary functions used to construct the input signal. The vector $\mathbf{m}\equiv\cup_{j=1}^{N}\{A_j,a_j,t_j\}$ is the set of parameters to be optimized and is really the hidden model to be inverted. A large choice of elementary functions Ψ is possible, and in the present study we use elementary functions Ψ belonging to the class of the wavelets with constant shape (e.g., Holschneider, 1995) and defined as

$$\Psi(t)=\frac{d^n}{dt^n}\exp(-\pi t^2). \tag{2}$$

These wavelets are bandpass functions with a peak frequency depending on the value of dilation a_j: the smaller the dilation, the higher the frequency. The bandwidth is controlled by the derivation order n. Examples of wavelets corresponding to $n=1$, 2, 3, and 4 are shown in Fig. 3. In this study, wavelets with $n=1$ are used to construct the input signals. Surprisingly, even when $N\simeq 10$ in Eq. (1), a sufficiently large subspace of input signals is generated to contain the optimized input signals giving the desired response signals. The possibility to use a hidden model dramatically reduces the number of model parameters (e.g., dim $\mathbf{m}=30$ for $N=10$) and strongly speeds up the convergence toward high-probability input models.

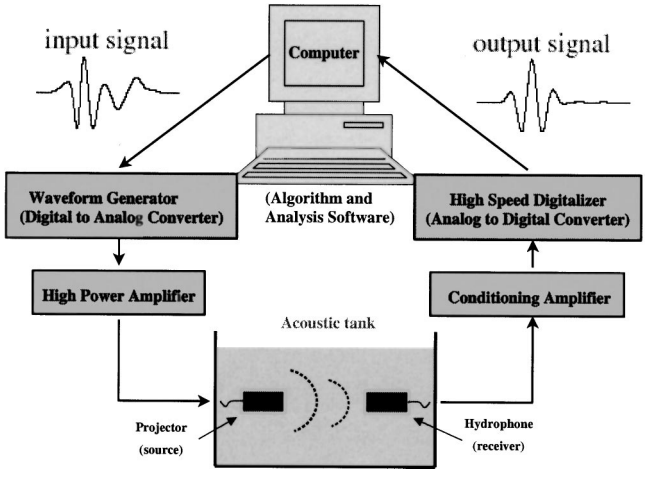

FIG. 2. Synoptic view of the experimental setup used in the present study. The source line is shown on the left part of the figure and is made of an arbitrary waveform generator, a power amplifier, and a source transducer (projector). The receiver line is shown on the right part of the figure and is made of a receiving hydrophone, a preamplifier, and an A/D converter. Both lines are connected to a computer which hosts both the simulated annealing algorithm and the driving softwares of the apparatus.

B. Probabilistic inversion

In the present paper, we consider the problem of input signal synthesis as an inverse problem formulated in a probabilistic form (Tarantola, 1987). With this approach the optimization procedure consists in searching for the models $\mathbf{m}$ with the largest posterior probability,

$$\rho(\mathbf{m})=M(\mathbf{m})S(\mathbf{m})R(\mathbf{m}), \tag{3}$$

where M is the prior probability density of $\mathbf{m}$, and S and R are probability densities which quantify the acceptability of $\mathbf{m}$ with respect to the corresponding signals $s(t|\mathbf{m})$ and $r(t|\mathbf{m})$.

When the constraints concerning the response signal $r(t|\mathbf{m})$ are given as a reference signal $r_r(t)$ to be fitted, the probability density $R(\mathbf{m})$ explicitly depends on the misfit between $r_r(t)$ and $r(t|\mathbf{m})$. The most classical definitions use the least-squares L_2 misfit,

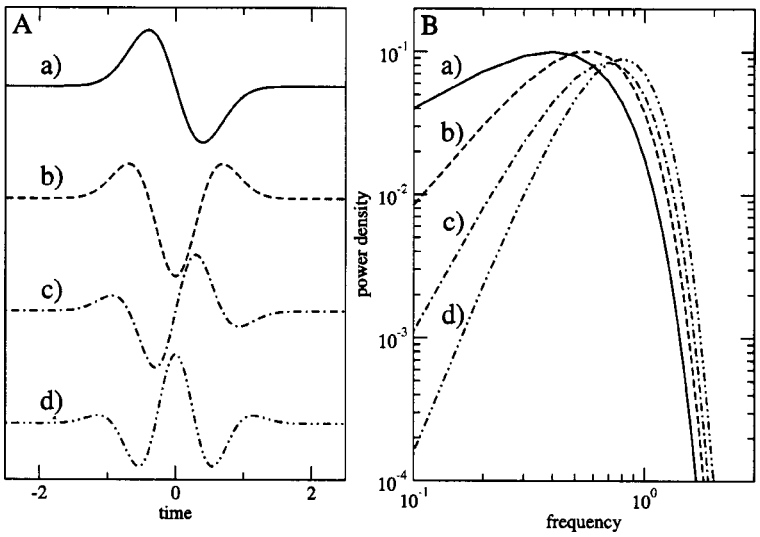

FIG. 3. A: Examples of elementary wavelets defined as the first (a), second (b), third (c), and fourth (d) derivatives of a Gaussian function. The wavelet (b) is also commonly referred to as the "*Ricker*" wavelet in seismic and as the "*Mexican hat*" wavelet in the wavelet literature. B: Power spectra of the wavelets shown on the left part.

$$R(\mathbf{m}) \equiv \eta \exp\left[-\int \frac{(r(t|\mathbf{m}) - r_r(t))^2}{2\sigma^2(t)} \mathrm{d}t \right], \tag{4}$$

or the more robust L_1 misfit,

$$R(\mathbf{m}) \equiv \eta \exp\left[-\int \frac{|r(t|\mathbf{m}) - r_r(t)|}{\sigma(t)} \mathrm{d}t \right], \tag{5}$$

where η is a normalization constant and $\sigma(t)$ is a "standard deviation" function which controls the degree of misfit tolerance. These definitions may account for variable fit constraints depending on which part of the response signal is considered. For instance, one may impose the response $r(t|\mathbf{m})$ to tightly fit the beginning of the reference signal $r_r(t)$ while a less-tight fit is acceptable in the remaining part of the signal. In other situations the constraints to be satisfied by the response signal may be defined in a more fuzzy manner so that the probability functions (4) and (5) are no more valuable. This may, for instance, be the case if the constraints on the response signal only concern its sign and its total duration T. An example of probability density accounting for these constraints may be

$$R(\mathbf{m}) \equiv \eta \exp\left[-\int_0^T [\mathrm{sign}(r(t|\mathbf{m})) - \mathrm{sign}(r_r(t))]^2 \mathrm{d}t - \int_T^\infty r^2(t|\mathbf{m}) \mathrm{d}t \right]. \tag{6}$$

In a similar manner, the probability function $S(\mathbf{m})$ is used to measure the acceptability of $\mathbf{m}$ with respect to its input signal $s(t|\mathbf{m})$. Contrary to the case of the response signal on which tight constraints can be applied, the precise form of the input signal is generally not important and the constraints are less hard. These may, for instance, be bounds on the amplitude of the signal or imposed limits on the total dissipated power in order to protect the apparatus against overload and failure.

The prior probability $M(\mathbf{m})$ may be used to control the complexity of the model and, in particular, to reduce the nonuniqueness of the solution and eliminate the components Ψ_j of $s(t|\mathbf{m})$ which belong to the null-space of the physical system, i.e., such that they produce a null response. As will be seen in a next section, reducing the nonuniqueness may be of some interest to construct a family of input signals further used to train neural networks. Indeed, the presence of unnecessary components in the optimized model results in a randomization of the training ensemble which may considerably alter the convergence of the neural net parameters during the training phase. In the present study, when used, the prior probability is simply defined as the inverse of the number of non-null components of the model $\mathbf{m}$,

$$M(\mathbf{m}) = \frac{1}{\dim\{A_j \neq 0\}}. \tag{7}$$

Our probabilistic formulation of signal synthesis allows us to freely define the imposed constraints to be satisfied by both the input and the response signals. This freedom results in a highly nonlinear influence of the model parameters which, together with the fact that the response of the physical apparatus is unknown and also nonlinear, eliminates the possibility to use classical optimization methods like steepest descent. Furthermore, these methods generally involve the Hessian matrice or the Fréchet's matrice of the partial derivatives $\partial r(t|\mathbf{m})/\partial m_k$ which are not easy (but not impossible) to evaluate for physical systems.

C. The Metropolis algorithm

The Metropolis algorithm (Metropolis *et al.*, 1953) is a Markov Monte Carlo chain which generates a sequence of models $\{\mathbf{m}_l\}$ distributed according to a prescribed probability density function ρ. The sequence is constructed as follows. Let $\mathbf{m}_l$ be the last model in the sequence, and let $\mathbf{m}_?$ be a candidate model to eventually become the next model $\mathbf{m}_{l+1}$. Then, the candidate model is retained and enters into the Metropolis sequence according to the following stochastic rules:

$$\mathbf{m}_{l+1} = \mathbf{m}_? \quad \text{with probability} \max\left[1, \frac{\rho(\mathbf{m}_?)}{\rho(\mathbf{m}_l)}\right], \tag{8}$$

$$\mathbf{m}_{l+1} = \mathbf{m}_l \quad \text{instead.} \tag{9}$$

These equations indicate that the candidate model $\mathbf{m}_?$ is eventually accepted with probability $\rho(\mathbf{m}_?)/\rho(\mathbf{m}_l)$ if $\rho(\mathbf{m}_?)$

$<\rho(\mathbf{m}_l)$ and is systematically accepted if $\rho(\mathbf{m}_?)\geqslant\rho(\mathbf{m}_l)$. The Metropolis sequence is iteratively constructed by randomly generating candidate models and by using the selection formulas (8) and (9). It can be shown that the models forming the so-constructed sequence are sampled according to the probability density ρ (Bhanot, 1988).

D. Simulated annealing

Simulated annealing (Kirkpatrick *et al.*, 1983) is a global search algorithm aimed at converging toward high-probability models for nonconvex, and even fractallike, posterior probability functions. The basic idea of simulated annealing is to iterate the Metropolis algorithm while controlling the topology of the posterior probability density function in order to progressively transform the sequence of models from a uniformly sampled one to a sequence of models confined in the vicinity of the global maximum of the posterior probability function. Since the precise topological characteristics of the probability density remain unknown, the topological deformation must rely on very general principles. For the simulated annealing algorithm, this is done through the use of a control parameter T, called the temperature for historical reasons, which is varied from infinity to 1. Practically, the topological transformation of the posterior probability reads

$$\rho_T(\mathbf{m})=\frac{1}{G}\rho^{1/T}(\mathbf{m}), \tag{10}$$

where ρ_T is the transformed posterior probability density for temperature T, and G is a normalization constant (in fact the partition function). Asymptotically ρ_∞ tends toward the uniform probability density, and for $T\downarrow 0$ we have $\rho_0\rightarrow\delta(\mathbf{m}-\mathbf{m_{MP}})$ where $\mathbf{m_{MP}}$ is the model with the maximum posterior probability.

Simulated annealing consists in iterating the Metropolis algorithm while decreasing the temperature T from a high value to 1. Provided the temperature is sufficiently slowly decreased, the sequence of models $\{\mathbf{m}_j\}$ progressively concentrates in the regions with high posterior probability. For this guidance to be efficient, some correlation is necessary among the nearby models of the sequence in order to perform a random walk rather than a random sampling in the model space. This is particularly true at low temperature where a pure Monte Carlo sampling would be very inefficient because of a too high rate of rejection of the tested models in the Metropolis loop. In the present study, the correlation among the models is done by two ways. First, as usually done in simulated annealing, the tested models $\mathbf{m}_?$ are generated by stochastically perturbing the last accepted model $\mathbf{m}_j$, i.e., by only modifying a subset of the model parameters. Second, the range of allowed changes for the model parameters is narrowed as the temperature decreases. This approach proved particularly efficient when dealing with continuous variables, as in the present study (Vanderbilt and Louie, 1984). In the present study, we implemented this method by performing a statistical analysis of the model sequence generated at each temperature during the annealing process. From this analysis the ranges of variation of the model parameters are progressively narrowed and centered on the region of high posterior probability $\rho(\mathbf{m})$ where the models cluster. This procedure considerably accelerates the convergence. Since the Metropolis uses the ratio of probabilities [see Eqs. (8) and (9)], the normalization constant G in Eq. (10) may be omitted and the probability distribution of the models in the Metropolis sequence may be *a posteriori* normalized.

III. EXPERIMENTAL NONLINEAR SYNTHESIS OF INPUT SIGNALS

A. Experimental setup

The experimental setup is shown in Fig. 2 and is composed of electronic devices, piezoelectric transducers, and a water tank of 5 m^3. All devices are remotely controlled by a master software written in LabView® language. First, the last model $\mathbf{m}_l$ of the Metropolis sequence is perturbed to give the candidate model $\mathbf{m}_?$ used to compute a discretized version of the input signal $s(t|\mathbf{m}_?)$ which is sent into the arbitrary waveform generator. Next, the analog physical electrical signal corresponding to s is created by the generator and entered in the power amplifier connected to the source transducer which produces an acoustical wave. Next, the acoustical wave reaches the piezoelectric receiver which is connected to a preamplifier and to a digital oscilloscope which sends a discretized version of $r(t,\mathbf{m}_?)$ to the computer. Finally, the response signal is used to compute $R(\mathbf{m}_?)$ and the posterior probability $\rho(\mathbf{m}_?)$ used in the Metropolis decision rules (8) and (9). After either $\mathbf{m}_?$ or $\mathbf{m}_l$ became the new last model $\mathbf{m}_{l+1}$ in the Metropolis sequence, a new candidate model is again created and the whole procedure is repeated. A real-time control of the simulated annealing process is done by plotting $r(t,\mathbf{m}_{l+1})$, $r_r(t)$, and $\rho(\mathbf{m}_{1,\ldots,l+1})$ in a LabView® window. This display of the intermediate results of the optimization process is useful to observe the efficiency of the cooling schedule in the simulated annealing loop.

B. Synthesis of input signals for an imposed response

In this first example, several input signals are inverted to produce a unique given response signal at a fixed source power. Figures 4(a) and (b) show the results of five inversions obtained with the constraint on the response signal given as an imposed reference signal $r_r(t)$ chosen to be the wavelet shown in Fig. 3(d). Both $M(\mathbf{m})=1$ and $S(\mathbf{m})=1$ in this example and the probability density $R(\mathbf{m})$ has the form given by Eq. (4) with a constant σ. As can be seen, the obtained input signals have conspicuous differences [Fig. 4(a)] while their corresponding responses remain identical [Fig. 4(b)]. These results illustrate the fact that the physical system, i.e., the forward problem in the inverse problem terminology, possesses a nonempty null-space containing input signals whose response is zero. These null-space elements have a frequency content so out-of-bandwidth that no response signal is produced by the physical system. Another form of nonuniqueness, but nonvisible in this example, is due to the fact that a single wavelet in the synthesis formula (1) may be replaced by two or more wavelets having the same dilation a_j and time position t_j. This first example

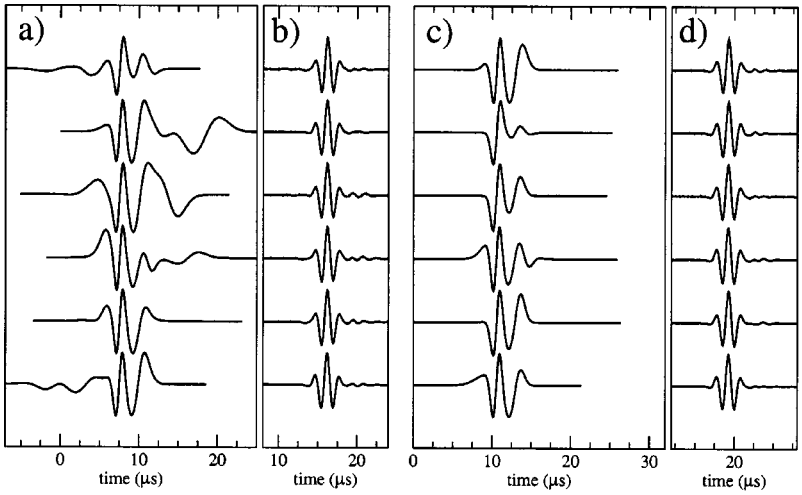

FIG. 4. Results of inversions performed for a unique given reference signal and a fixed source power. (a) Input signals inverted with both $M(\mathbf{m})=1$ and $S(\mathbf{m})=1$. (b) Corresponding response signals. (c) Input signals inverted with $M(\mathbf{m})$ given by Eq. (7). (d) Corresponding response signals.

shows that a given arbitrary response signal may be obtained with a good quality. The fact that this response may be produced by rather different input signals is generally not a problem and illustrates the ill-posedness of deconvolution. However, there may be particular instances where it is desirable to reduce nonuniqueness when inverting a family of input signals. Figure 4(c) shows the inverted signals equivalent to those of Fig. 4(a) but obtained by using the prior probability $M(\mathbf{m})$ given by Eq. (7). As can be seen, this additional constraint strongly reduces the discrepancies among the inverted input signals without altering the quality of the corresponding response signals [Fig. 4(d)]. Slight discrepancies between the output signals may be observed particularly in their coda parts where tiny wiggles appear in some outputs. These oscillations remain in the obtained solutions because the input model $\mathbf{m}$ has a limited number of wavelets Ψ_j which concentrate in the early part of the input signal $s(t|\mathbf{m})$ in order to correctly reproduce the main part of the desired output signal. If unwanted, these artifacts could be suppressed by using a more complicated input model with a sufficiently large number of wavelets Ψ_j so that a longer and more adapted input signal could be constructed by simulated annealing.

Figure 5 shows the annealing process observed during an inversion. The posterior probability $\rho(\mathbf{m})$ of the models accepted during the Metropolis loops may be very low when the temperature parameter is high at the beginning of the iterative procedure. This stage of the annealing is critical for it allows a global search among the model space and important changes of the parameter values. This is possible because at this stage of the process the random walk in the model space may go through very low probability models in order to eventually escape from local maxima of the posterior probability. It is important that the global search can quickly explore large parts of the model space in order to localize the region with the global maximum of probability. This region is identified by performing a statistical analysis of the models accepted during each successive Metropolis loop in order to see where the accepted models progressively cluster. Once the region with the global maximum is identified, the posterior probability of the accepted models drops suddenly when the temperature decreases [around iteration number 20 in Fig. 5(a)], and we observe that the remaining iterations of the annealing procedure are restricted to a subregion of the model space. It is, however, necessary to continue the annealing procedure with a sufficiently slow cooling in order to gently guide the model sequence toward the global maximum. We observe that a too-rapid decrease of the temperature traps the models into a local maximum.

C. Synthesis of input signals for different source powers

The examples presented in this section concern the synthesis of the input signals producing a given response wavelet for the same power levels as in Figs. 1(a) and (b). As in the preceeding section, the constraint on the response signal is given as a reference signal and the nonuniqueness is reduced by using the prior probability $M(\mathbf{m})$ given by Eq. (7). The inverted input signals are shown in Fig. 1(c) and display subtle differences to account for the nonlinearities of the physical system. The corresponding response signals are shown in Fig. 1(d) and look very identical as expected.

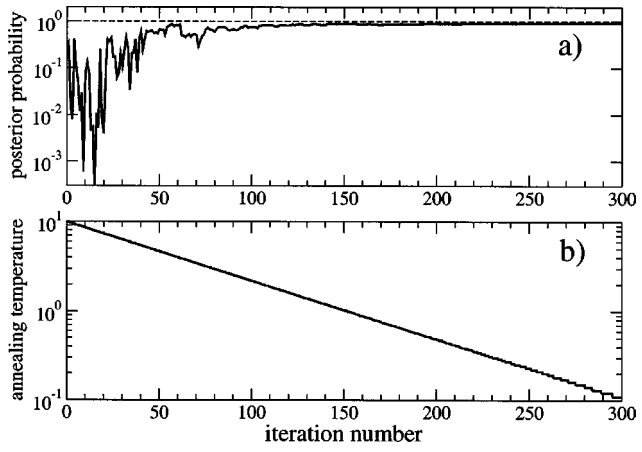

FIG. 5. (a) Posterior probability $\rho(\mathbf{m})$ of the models accepted during an annealing sequence with a temperature schedule given by $T_{k+1}=0.985T_k$ in part (b) of the figure. Each iteration counts 20 model tests at a fixed temperature, so the 300 iterations shown here correspond to 6000 tested (and eventually accepted) models. In practice, this takes about 10 min to be performed.

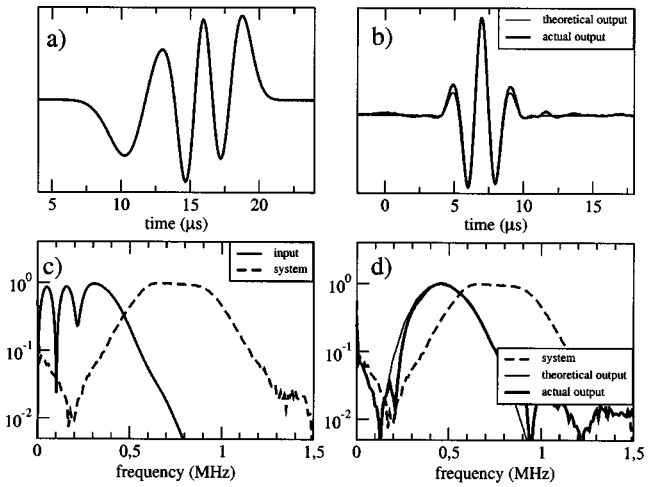

FIG. 6. Synthesis of input signals out of the main frequency band of the system. (a) Optimized input signal. (b) Actual response signal and reference response signal. (c) Spectral amplitude of the optimized input signal shown in (a). (d) Spectral amplitude of the response signals (both actual and reference) and of the impulse response of the physical system.

D. Synthesis out of the main frequency band

An interesting feature of the proposed algorithm is that it allows us to find input signals whose response signals have a frequency content partly out of the nominal bandwidth of the physical system. This possibility is particularly useful to construct a family of response signals covering a wide frequency bandwidth. Even when the physical system operates in a linear regime, classical deconvolution methods using an impulsive input signal do not produce satisfactory results concerning the out-of-bandwidth responses. This is because most of the energy of the input impulse is released at the central bandwidth of the system, rejecting the useful bandwidth at the noise level. A great interest of our method is that the input signals are constructed in such a manner that energy is sent only at the relevant frequencies so that no saturation occurs due to strong energy release in the dominant frequency band. Figure 6 shows the results of such an inversion. One can observe that the algorithm is able to find an input signal whose corresponding response has a spectral content out of the central bandwidth of the physical system. This can be obtained by producing an input signal with almost no energy located in the central band and such that a high signal-to-noise ratio is obtained.

E. Synthesis of a wavelet family

The proposed method allows us to generate families of signals optimally located in the time-frequency domain, as shown in Fig. 7, where the response signals are dilated versions of the wavelet (d) in Fig. 3. In this example, four pairs of transducers with central frequencies of 250, 500, 750, and 1000 kHz were used, and the frequency range covered by the whole set of signals goes from 150 kHz to 1.2 MHz. Such a family of signals is useful to study the frequency response of a part of a complex system. Indeed, in this kind of situation, it is necessary to extract the response of the studied system element from a complex and intricate global response. This extraction is generally impossible when the frequency response is studied through the classical Fourier approach by using sinusoidal input signals with a long duration. Conversely, using a wavelet family as shown in Fig. 7 allows us to obtain an ensemble of responses of the system with good time-frequency properties. The time localization of the signals enables a temporal separation of the response of subsystems of interest while controlling the time-frequency characteristics of the signals.

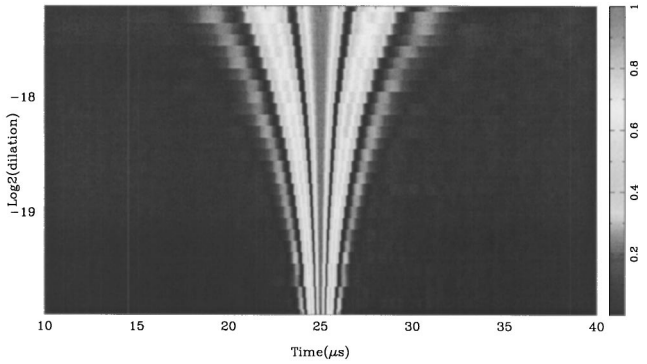

FIG. 7. Output wavelet family corresponding to a collection of inverted input signals constrained to produce dilated versions of the wavelet shown in Fig. 3(d). Each line of the color array represents a wavelet whose absolute value is coded according to the color scale shown on the right. The dilations are such that $a=f_c^{-1}$ where f_c is the central frequency of the response signal given in Hz.

F. Application: Reflectivity study of granular media

We now give an example of application of the wavelet family shown in Fig. 7. The objective of the experiment is to study the frequency dependence of the reflectivity of the surface of a layer of disordered monodisperse glass beads (see Le Gonidec *et al.*, 2002, 2003 for details). The experiment consists in recording the spatially averaged wavefield reflected by the surface in response to the incident wavelets of Fig. 7. Figure 8 shows the spatially averaged reflected signals corresponding to the input signals of the wavelet family. The time origin of each averaged signal has been arbitrarily shifted in order to align the second extrema of all signals. At large dilations (i.e., large wavelengths) the reflected signals are arranged as a conical structure which converges toward the average time-location of the surface of the heterogeneous

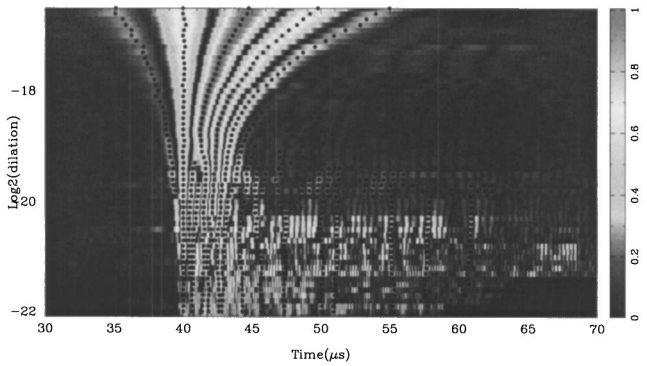

FIG. 8. Modulus of the average coherent signal reflected by a layer of glass beads in response to the incident wavelets shown in Fig. 7. The dilations are such that $a=f_c^{-1}$ where f_c is the central frequency of the response signal given in Hz.

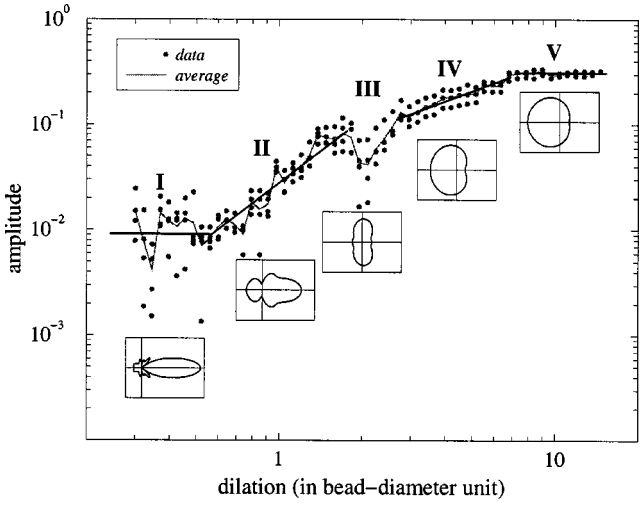

FIG. 9. Reflectivity of the layer of glass bead inferred from the amplitude of the coherent reflected signals shown in Fig. 8. See Le Gonidec *et al.* (2002, 2003) for details.

layer. At smaller dilations (i.e., shorter wavelengths) the main cone of the wavelet response is followed by a coda, and the time localization of the reflector is blurred. The frequency dependence of the reflectivity may be accurately studied by plotting the amplitude of the reflected wavelets against the wavelength normalized by the bead diameter (Fig. 9). At wavelengths larger than seven times the bead diameter (waveband V in Fig. 9) the reflectivity is constant and the heterogeneous layer behaves like a homogeneous elastic effective medium, while at smaller wavelengths (waveband IV) some attenuation occurs due to increasing scattering. The waveband III marks a transition and corresponds to a sharp decrease of the reflectivity. Physically, this narrow waveband corresponds to dominant transverse Mie scattering while backscattering dominates in bands IV and V. The reflectivity decrease in band III may then be explained by the fact that a significant fraction of the incident wave is laterally scattered out of the coherent reflected wave. Band II displays a sharper decrease of the reflectivity when the wavelength shortens. This corresponds to a dominant forward Mie scattering where more and more energy is scattered forward in the heterogeneous layer, contributing to the conspicuous coda visible in Fig. 8. In band I corresponding to the shortest wavelengths, equal to or shorter than the bead radius, the coherent reflected signal is caused by the water–glass interface, and the reflectivity is more the one of the rough water–glass interface than the one of the heterogeneous as a whole (Le Gonidec *et al.*, 2002, 2003).

We emphasize that these experimental results are directly obtained without postprocessing deconvolution. Once the wavelet family is obtained, the corresponding input signals are sent to the source chain and the reflected signals are averaged and recorded as shown in Fig. 8. The methods allows for a tight control of the shape of the desired response signals so that the reflectivity may be accurately determined.

IV. CONCLUSION

The nonlinear method presented in this paper performs a Monte Carlo search of the input signals able to produce a desired signal at the response of a nonlinear acoustical chain. This is done by simulated annealing which guides a random walk through the model space. This may be done by embedding the physical system in the operating software by using fast A/D converters. The main advantages of the proposed method are (1) the possibility to generate a unique given signal for various source power by accounting for the nonlinear distortions occurring in the physical system (Fig. 1); (2) the possibility to generate response signals with a frequency content located out of the nominal bandwidth of the system (Fig. 6); and (3) the possibility to perform an optimal time-frequency analysis and to isolate individual responses from composite responses involving different physical phenomena (Fig. 8).

ACKNOWLEDGMENTS

Yves Le Gonidec kindly gave us the data of the wavelet response example. Arnaud Derode gave us much valuable advice and generously shared his experimental and theoretical knowledge. This work is financially supported by the CNRS and ANDRA through the GdR FORPRO (Research Action No. 99.II) and corresponds to the GdR FORPRO Contribution No. 2003/02 A.

Bhanot, G. (**1988**). ''The Metropolis algorithm,'' Rep. Prog. Phys. **51**, 429–457.

Bendat, J., and Piersol, A. G. (**1971**). *Random Data: Analysis and Measurement Procedure* (Wiley Interscience, New York).

Gautier, S. (**2002**). ''Imagerie Acoustique de Discontinuités Rugueuses: Expérimentation et Modélisation Numérique'' (''Acoustical Imaging of Rough Discontinuities: Experiments and Numerical Modeling''), Ph.D. thesis, University Rennes 1.

Gautier, S., and Gibert, D. (**2003**). ''Scattering from a fractal surface: Acoustical experiments and comparison with near-nadir models,'' Icarus (in press).

Holschneider, M. (**1995**). *Wavelets: An Analysis Tool* (Clarendon, Oxford, England).

Jurkevics, A., and Wiggins, R. (**1984**). ''A critique of seismic deconvolution methods,'' Geophysics **49**, 2109–2116.

Kirkpatrick, S., Gellatt, C. D., and Vecchi, M. P. (**1983**). ''Optimization by simulated annealing,'' Science **220**, 671–680.

Le Gonidec, Y. (**2001**). ''Caractérisation d'Interfaces et de Milieux Complexes par Analyse Sismique Multi-Échelle: Expérimentation et Modélisation Numérique'' (''Interfaces and Complex Media Characterization by Multi-scale Analysis: Experiments and Numerical Modeling''), Ph.D. thesis, University Rennes 1.

Le Gonidec, Y., Conil, F., and Gibert, D. (**2003**). ''The wavelet response as a multiscale NDT method,'' Ultrasonics, **41**, 487–497.

Le Gonidec, Y., Gibert, D., and Proust, J.-N. (**2002**). ''Multiscale analysis of waves reflected by complex interfaces: Basic principles and experiments,'' J. Geophys. Res. **107**(B9), 2184.

Metropolis, N., Rosenbluth, A., Rosenbluth, N., Teller, A., and Teller, E. (**1953**). ''Equation of state calculations by fast computing machines,'' J. Chem. Phys. **21**, 1087–1092.

Tarantola, A. (**1987**). *Inverse Problem Theory* (Elsevier, New York).

Trucco, A. (**2002**). ''Weighting and thinning wide-band arrays by simulated annealing,'' Ultrasonics **40**, 485–489.

Vanderbilt, D., and Louie, S. G. (**1984**). ''A Monte Carlo simulated annealing approach to optimization over continuous variables,'' J. Comput. Phys. **56**, 259–271.